Journal of Rehabilitation in Civil Engineering 8-2 (2020) 62-80

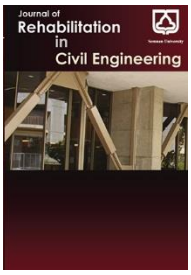

journal homepage: http://civiljournal.semnan.ac.ir/

Seismic Damage Assessment of RC Buildings Subjected to the Rotational Ground Motion Records Considering Soil-Structure Interaction

M.B. Payganeh[1] and A. Mortezaei[2*]

1. M.Sc. Graduate of Structural Engineering, Civil Engineering Department, Semnan Branch, Islamic Azad University, Semnan, Iran

2. Associate Professor, Seismic Geotechnical and High Performance Concrete Research Centre, Civil Engineering Department, Semnan Branch, Islamic Azad University, Semnan, Iran

Corresponding author:*a.mortezaei@semnaniau.ac.ir*

ARTICLE INFO

Article history:
Received: 13 March 2019
Accepted: 10 October 2019

Keywords:
Rotational Component,
Soil-Structure Interaction,
RC Moment-Resisting Frame,
Nonlinear Dynamic Analysis.

ABSTRACT

The significance of the seismic rotational components have been overlooked in the seismic evaluation of structural behavior. As researchers have measured seismic components more accurately using sensitive rotational velocity sensor, it was observed that the magnitude of rotational components is considerable and could not be neglected. Hence, some parts of seismic damage or failure of structures cannot be exclusively attributed to the translational components. In this regard, this paper used seven accelerograms in which rotational components were measured by advanced sensors. The considered RC buildings which designed as per intermediate moment-resisting frame system were analyzed using OpenSees in nonlinear dynamic domain. In the numerical modeling, lumped plasticity model was used to simulate the behavior of RC component members considering the rotational motions and soil-structure interaction as main parameters. The results of numerous nonlinear time history analyses showed that the contribution of rotational components to the seismic behavior of RC frames is considerable and should be included in the seismic design codes.

1. Introduction

The earthquake ground motion is highly related to two or three translational components which are used typically in seismic analysis, design and performance assessment of buildings, bridges and safety-related nuclear structures. The effect of rotational components (rocking and torsional) is still vague since accelerographs deployed in the free field are not able to measure their intensity and frequency content, although they contribute to the response and damage of these structures

DOI: 10.22075/JRCE.2019.17206.1319

significantly. Typical seismic design and performance assessment do not take in to account the rotational motions. It is possible that rotational components be measured either directly or using robust procedures to extract the rotational time series from translational ones.

Richter [1] stated that rotations about three perpendicular axes must be considered, therefore three more instruments would be needed if a perfectly general motion is required. However, such rotations are not negligible according to the theory and observation. It is obvious that there were no instruments to measure the rotational motions with high level of sensitivity at that time. According to Aki and Richards [2], the latest technology at that time lack of sufficient sensitivity to be useful in geophysical application. Aki and Richards [3] stated later that in spite of utility of measuring device near a rupturing fault plane, the seismologist still await for a suitable device of measuring rotational motions.

In 1990s, Nigbor recorded the rotational ground motions near a large explosion at the Nevada Test Site using a Gyro Chip rotational sensor [4]. In addition, Takeo, using similar instruments, recorded these motions during an earthquake in Izu Peninsula of Japan [5].

Examining 50 near-field strong motions which recorded along 100 km rupture in 1999 Chi-Chi earthquake showed that the recorded ground motions are so complex [6]. It was so hard double integrating the acceleration data to achieve displacements that were independently observed by geodesy, without some baseline corrections or high-pass filtering. A peak rotation velocity of 0.4 mrad/sec was reported by Huang, using the records from a dense acceleration array on the Li-Yu-Tan Damin Chi-Chi earthquake fault rupture [7].

Liu et al. [8] deployed a far more sensitive rotational velocity sensor (K2+R1) at the HGSD station in eastern Taiwan. From 2007 to 2008, 52 local earthquakes with good rotational velocity signals were observed together with excellent translational acceleration signals.

Falamarz-Sheikhabadi [9] presented the acceleration response spectra of rocking and torsional components. He showed that the contribution of earthquake rocking components to the rotational loading of multistory buildings is strongly sensitive to structural irregularity, structural height, and seismic excitation.

Basu et al. [10] developed a new procedure known as Surface Distribution Method (SDM) for extracting rotational components from recorded translational data.

Since at the large hypocentral distances, it is convenient to approximate the curved transient seismic wave-fronts as planar to estimate rotational ground motions from the single-station recordings of translational ground motions, Singla and Gupta [11] investigated whether and when the plane-wave approximation can be considered adequate close to the source. They concluded that the plane-wave approximation might be acceptable when the wave-lengths of the seismic waves are much smaller than the source depth.

Falamarz-Sheikhabadi and Ghafory-Ashtiany [12] addressed the rotational loading pattern of multi-storey buildings supported by spread and continuous interconnected single foundations. The results showed that the

influence of the seismic loading of the rotational components on the upper parts of the tall buildings is larger than that of the lower parts. Relying on their results, as the rotational motions have more high-frequency content than the translational ones, the foundation input rotational components are more dependent on the effects of the kinematic soil–structure interaction.

Literature review show that there have been limited studies in this area, and most of these studies have focused on fixed-base structures [13-16]. Input ground motion for a structure is usually based on the free-field excitations.. If a structure is built on hard soil, the dynamic analysis under free-field excitation is an appropriate analysis. In this case, the inertial forces in the structure are unable to cause further deformations in structural base. On the contrary, flexibility of the structural base, i.e. soft soil environment, will affect input ground motion and structural response by the soil-structure interaction (SSI). The effects of soil-structure interaction can be divided into two parts, namely kinematic interaction and inertial interaction.

Since the impact of rocking as well as horizontal components in structural response is significant, it should be included in seismic analysis and design. In this regard, this paper uses seven accelerograms in which rotational components were measured by advanced sensors in HGSD station of eastern Taiwan. The considered RC buildings which designed as per intermediate moment-resisting frame system are analyzed using *OpenSees* in nonlinear dynamic domain considering soil-structure interaction.

2. Methodology

2.1. Model Properties

In this paper, three primary models of 5-, 10-, and 15-story frames are selected as the structural models. The models are firstly analyzed and designed based on Iranian Code of Practice for Seismic Resistant Design of Buildings (Standard No. 2800) [17] and Iranian National Building Code, Part 9 [18]. In order to do nonlinear dynamic analysis, the models are then simulated in *OpenSees* software. The lateral load-bearing system is assumed and detailed as intermediate moment-resisting RC frames like typical buildings. The plan form of structure is rectangular and the elevation view is in the longitudinal direction as shown in Figure 1. The height of each floor is assumed to be 3.2 m. The weight of structural members consists of normal weight of concrete as well as the compressive strength of 25 MPa and nominal yield strength of steel reinforcement of 400 MPa.

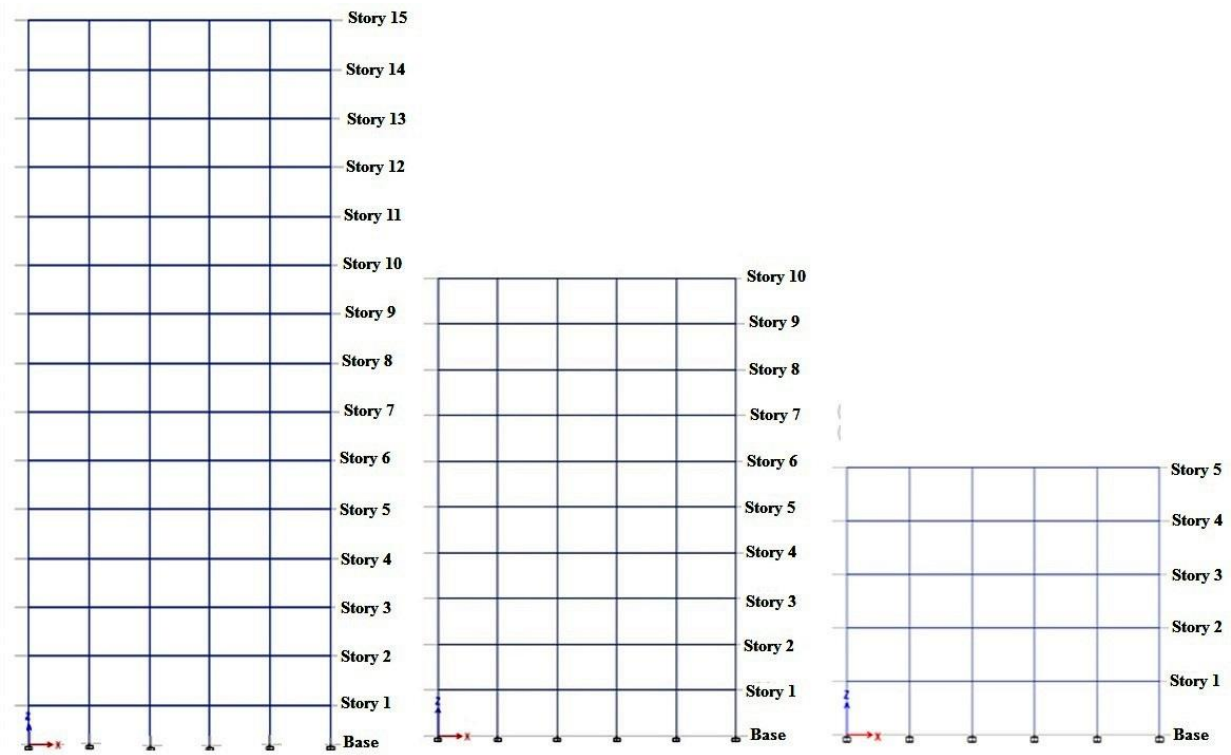

Fig. 1. Elevation view of the selected models.

The building models are assumed to be located in an area with soil type III and most seismically active zone (A=0.35g), as per the Iranian Code of Practice for Seismic Resistant Design of Buildings [17]. The dead load and live load of all stories are assumed to be550 kg/m^2 and 200 kg/m^2, respectively. The contribution of live load in determining the seismic effective mass is 20 percent.

The 3D model was developed using commercially available software, ETABS2000 for primary analysis of buildings [19]. The model was generated according to the methods provided for multistory reinforced concrete structures [20]. All the beams were idealized as T-beams in order to take into account the effective width of the slab. The slab was modeled as rigid diaphragms to constrain all the nodes on each floor. To account for cracked section properties of all members, flexural stiffness modifiers of 0.35 were applied to the gross cross-section of the beams while the values of 0.7 were used for the columns. Table 1 shows the frame element details, i.e. dimensions and reinforcements, in selected models.

2.2. Selected Rotational Ground Motion

Seven real ground motion records, listed in Table 2. The selected rotational ground motions were recorded from a dense acceleration array near the northern end of the rupture fault in the 1999 Chi-Chi, Taiwan earthquake. Major frequency content is from 0.1 to 1.0 Hz with a peak near 0.2 Hz.

Table 1. Frame element details of selected models.

Story	5-story models			10-story models			15-story models		
	Columns	Beams	Top R. Bot R.	Columns	Beams	Top R. Bot R.	Columns	Beams	Top R. Bot R.
Story 01	50*50-16T22	40*30	2T18 2T16	50*50-16T18	40*30	3T20 2T20	60*60-16T22	40*30	3T20 2T20
Story 02	40*40-12T22	40*30	2T18 2T16	50*50-16T18	40*30	4T20 3T20	60*60-16T22	40*30	3T20 2T20
Story 03	40*40-12T22	40*30	2T18 2T16	50*50-16T18	40*30	4T20 2T20	60*60-16T22	40*30	3T20 2T20
Story 04	35*35-12T20	40*30	2T18 2T16	40*40-12T18	40*30	4T20 2T20	50*50-16T22	40*30	4T18 2T18
Story 05	35*35-8T20	40*30	2T18 2T16	40*40-12T18	40*30	3T18 2T18	50*50-16T22	40*30	3T18 2T18
Story 06				35*35-8T18	40*30	2T18 2T18	50*50-16T22	40*30	3T18 2T18
Story 07				35*35-8T18	40*30	2T18 2T18	45*45-12T20	40*30	3T18 2T18
Story 08				35*35-8T18	40*30	2T18 2T18	45*45-12T20	40*30	3T18 2T18
Story 09				35*35-8T16	40*30	2T18 2T18	45*45-12T20	40*30	3T18 2T18
Story 10				30*30-8T16	40*30	2T18 2T18	45*45-12T20	40*30	3T18 2T18
Story 11							35*35-12T18	40*30	3T18 2T18
Story 12							35*35-12T18	40*30	3T18 2T18
Story 13							35*35-8T16	40*30	3T18 2T18
Story 14							35*35-8T16	40*30	3T18 2T18
Story 15							35*35-8T16	40*30	3T18 2T18

Table 2. Selected rotational ground motions.

Number	Earthquake	Latitude (°)	Longitude (°)	Depth (km)	M_L	M_w	Distance (km)	PGA (m/s^2)	PRV (mrad/s)
1	Chi-Chi	23.72	121.64	38.6	5.77	5.07	51.1	0.474	0.634
2	Chi-Chi	24.28	122.25	54	6.63	6.17	132.8	0.469	0.523
3	Chi-Chi	23.31	121.46	28.3	5.43	5.03	34.9	0.322	0.494
4	Chi-Chi	23.57	121.55	32.7	4.95	4.38	36.1	0.219	0.353
5	Chi-Chi	23.3	121.57	37.6	4.91	4.08	45.6	0.088	0.093
6	Chi-Chi	23.57	121.54	33.1	4.23	3.63	36.1	0.072	0.098
7	Chi-Chi	23.42	121.52	21.5	3.97	3.5	24.9	0.07	0.095

Note: the hypocenter is given by latitude, longitude, and depth; M_L is local magnitude; M_w is moment magnitude; the distance measured is the hypocentral distance to the HGSD station in kilometers; PGA is the peak ground acceleration in m/sec^2; PRV is the peak rotational velocity in mrad/sec.

2.3. Nonlinear Behavior Analysis

The nonlinear time history analysis that consider both material and geometric nonlinearities of structures are commonly used for the nonlinear seismic response assessment. The nonlinearities are simulated during nonlinear direct-integration time history analysis available in OpenSees software [21]. In this study,concentrated plasticity method is used to model the

behavior of concrete members. This method considers the possibility of plastic joints exclusively in the ending points of members using a rotational spring reflecting joint moment-rotation behavior. Concentrated plastic hinges were assigned to the frame elements to account for the material nonlinearity. The geometrical nonlinearity was reflected during the nonlinear direct-integration analysis in conjunction with P-delta analysis provided by OpenSees software. The member behavior along two plastic joints was assumed to be completely elastic, which is represented by elastic beam-column elements.

Modeling of panel zone was carried out by *Joint2d* element [22]. Four nodes (as shown in Fig. 2) were used for introducing the element whose coordinates are defined based on the panel zone geometry. Shear behavior of the panel zone, which is assumed to be elastic, is allocated by a pre-defined material.

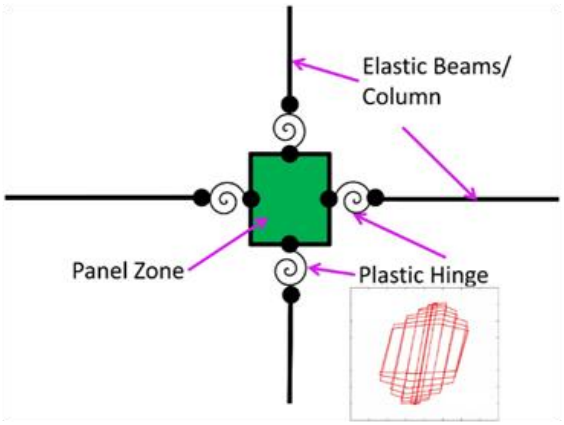

Fig. 1. Modeling the nonlinear behavior of the frame members using the concentrated plasticity method [22].

The rotational springs provided by *Joint2d* element were used for modeling the moment-rotation behavior of the ending points of beams and springs. The springs were placed at the node points of the element, and their allocated material, which is provided to the elements by their labels, represents moment-rotation behavior of the springs. Moment-rotation behavior of the springs was defined by the *Clough* material in *OpenSees* library. The material is based on the Ibarra-Krawinkler behavioral model [23] with the skeleton curve shown in Figure 3. The rotational behavior follows the peak-oriented model with cyclic deterioration of stiffness and strength as shown in Figure 4. The parameters used in defining the materials shown in Figure 5 which were proposed by Haselton [24] through the empirical relations obtained from experimental results. Figure 5 shows a sample calibration of the material parameters.

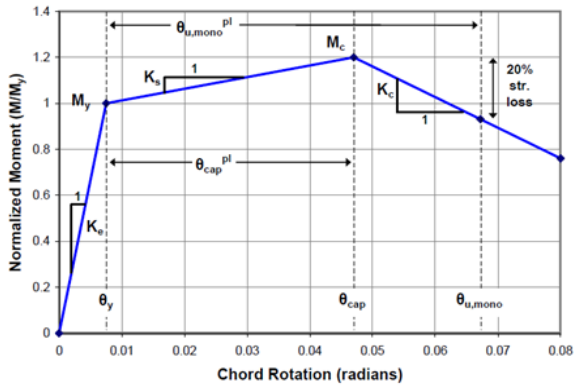

Fig. 2. The skeleton curve of the Ibarra-Krawinkler behavioral model [23].

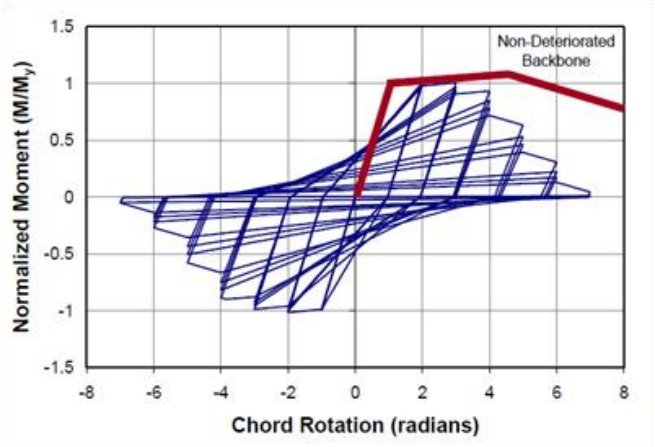

Fig. 3. Clough material skeleton curve with its cyclic behavior [23].

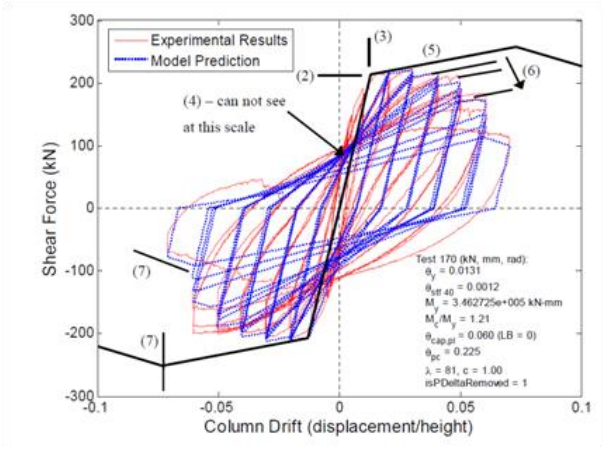

Fig. 4. A sample of calibration for Clough material based on experimental results [24].

2.4. Modeling of Soil and Soil-Structure Interaction

The middle frame of 3D structural model is considered with five spans in each direction.

Using the sub-structure method, the structure and the soil are modeled independently and then combined to constitute the soil–structure system. In this study lumped-parameter model (Cone model) is used to simulate supporting soil. In cone model, the soil is modeled as a homogenous half-space and substituted with a spring and dashpot system. A translational and a rotational spring are used to represent the sway and rocking degree-of-freedom. Also, viscous dampers are used to simulate energy dissipation of the soil because of radiation and material damping. The assumed coefficients of the soil model are:

$$k_h = \frac{8\rho V_s^2 r}{2-\nu} \quad c_h = \pi\rho V_s r^2$$

$$k_\varphi = \frac{8\rho V_s^2 r^3}{3(1-\upsilon)} \quad c_\varphi = \frac{\pi\rho V_p r^4}{4} \qquad (1)$$

where k_h, c_h, k_φ and c_φ are sway stiffness, sway viscous damping, rocking stiffness and rocking damping, respectively. ρ, υ, V_p and V_s are respectively the mass, Poisson's ratio and dilatational and shear wave velocities of soil [25].

By considering that the length of each span is 5 meters, the foundation of the 3D structural model is assumed to be square with the length of 27 meters to determine soil stiffness coefficients. The equivalent radius for sliding and rocking degrees of freedom is determined by Equation (1):

$$r_h = \sqrt{\frac{A}{\pi}} r_\varphi = \sqrt[4]{\frac{4I}{\pi}} \qquad (2)$$

where A is foundation area and I is moment of inertia of the foundation. According to the Equation (1) r_s and r_r are equal to $r_h = 15.233\ m$ and $r_\varphi = 15.41\ m$, respectively.

The effects of soil-structure interaction are considered in two different cases. In the first case, the shear wave velocity (V_s) and soil density (ρ) are 200 m/s and 1600 kg/m^3, respectively. In the second one, the shear wave velocity and soil density are 100 m/s and 1450 kg/m^3, respectively. Density values are determined based on similar V_s values and ATC-40 regulations [26]. The foundation is considered planar and rigid. The overall soil specifications are listed in Table 3.

Table 3. Overall soil specifications.

Specification	Value
Poisson's ratio (ν)	0.4
Hysteresis damping (ζ)	0.05
Buried depth of foundation (e)	0
Ground motion acceleration coefficient (A_v)	0.2

The modulus of elasticity of Soil (G) is determined as per Equation 2.

$$G = \rho V_s^2 \quad (3)$$

The shear modulus of elasticity is 64000 kN/m^2 and 14500 kN/m^2 for cases 1 and 2, respectively.

Sub-structure method is used for modeling soil-structure system, by which soil can be modeled separately and then combined for creating a soil-structure system. Soil-foundation element is modeled by the equivalent linear discrete model based on the cone model. Figure 6 shows a sample of the conventional models of shear buildings with fixed and flexible support systems. Translational and vibrational degrees of freedom are, defined as the representatives of translational and rotational motions of surface foundation, respectively, by overlooking the slight effect of vertical and torsional motions. The stiffness and energy loss of support soil are respectively shown by springs and dampers. Table 4 shows the translational and rocking stiffness and damping coefficients obtained from the aforementioned relations. Table 5 presents the period of the frames with fully fixed supports in the presence of soil. In this table, T_{fix} is the fundamental period of the rigid frame, and T is the fundamental period of the soil-structure system.

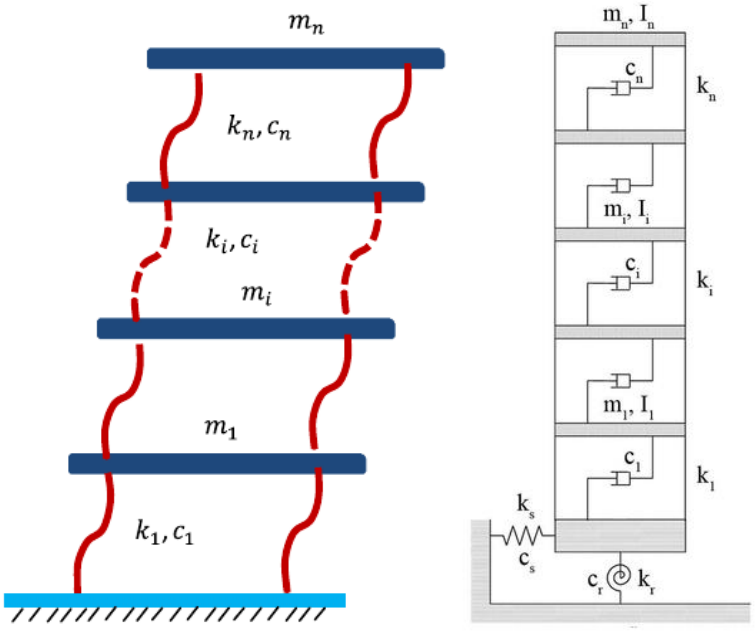

Fig.5. A sample of conventional models of shear structures with fixed and flexible support systems.

Table 4. Different parameters in soil modeling.

	ρ (kg/m^3)	V_s (m/s)	K_h (N/m)	K_φ (N/m)	c_h (N.Sec/m)	c_φ (N.Sec/m)
First scenario	1600	200	4874560000	1.04089E+12	233269482.8	14172210879
Second scenario	1450	100	1104392500	2.35827E+11	105700234.4	6421783055

- All values are in the SI system

Table 5. Structural period considering SSI.

	T_{fix} (sec)	T (sec)		T / T_{fix}	
		V_s=200 m/s	V_s=100 m/s	V_{so}=200 m/s	V_{so}=100 m/s
5 Story	1.0823	1.113	1.1743	1.028	1.085
10 Story	1.4215	1.5291	1.7313	1.07567	1.218
15 Story	2.0785	2.2941	2.6911	1.104	1.295

- All values are in the SI system

2.5. Park-Ang Damage Index Model

The Park-Ang damage model, which was introduced in 1985, is one of the most common damage indices for analyzing damage of structural members and, at larger scales, of structures [27]. By this model, damage index can be calculated in three levels of: member, story, and whole structure. Although this model was first used for determining damage of reinforced concrete members, it was then employee for evaluating damage of steel structures due to its obvious physical concept and convenient use. The Park-Ang damage index is expressed as a combination of maximum non-cumulative deformation and hysteretic energy based on Equation3, where δ_m, δ_u, Q_y, and $\int dE$ represent the maximum deformation of a member caused by the earthquake, ultimate deformation capacity, which can be resisted by a member (due to incremental loading effect), member yield stress, and the amount of dissipated energy in cyclic loading, respectively. β is the constant parameter of the model, indicating the effect of dissipated energy in damage.

$$DI = \frac{\delta m}{\delta u} + \frac{\beta}{Qy\delta u}\int dE \quad (4)$$

where $\int dE$ and δ_m are the parameters that depend on loading history, whereas the parameters β, δ_u, and Q_y are independent of loading history. It should be noted that "zero" (0) represents a healthy member/structure, while "one" (1) represents the complete collapse of an element or a structure [28]. Table 6 displays the categorization of damage modes and its relationship with the damage index.

Table 6. Classification of damage modes and its relationship with damage index.

Damage Modes	Without Damage	Low Damage	Repairable	Unrepairable	Complete collapse
Damage Index	DI< 0.1	0.1≤ DI< 0.25	0.25≤ DI< 0.4	0.4≤ DI< 1.0	DI≥ 1.0

In 1992, Kunnath *et al*. [29] modified the Ang-Park damage model as per Equation (5):

$$DI = \frac{\theta m - \theta y}{\theta u - \theta y} + \frac{\beta}{My\theta u}\int dE \quad (5)$$

In this model, cross-section rotation and yield moment were substituted by displacement and yield strength, respectively. In this equation, θ_y, θ_m, and θ_u represent yield rotation, maximum rotation, and maximum rotation capacity of a member when cross-section subject to a uniform incremental loading, respectively. The moment behavior of a reinforced concrete member is quite evident in the modified model.

To use this model, it is necessary to determine parameter β, which is related to strength deterioration. Park and Ang proposed an equation to calculate this parameter, in which the variables including shear span ratio, axial load, ratio of longitudinal reinforcing bars, and confining steel reinforcements ratio are effective. β shows the energy dissipation as a result of structural damage. In an experiments done by Park and Ang on beam and column specimens, they calculated the dissipated energy and proposed Equation (6) to determine coefficient β.

$$\beta = \left(-0.447 + 0.073\frac{l}{d} + 0.24n + 0.314\rho\right) \times 0.7^{\rho_w} \quad (6)$$

Where *1/d* is the shear span ratio, *n* is the normalized axial load, ρ is the percentage of longitudinal reinforcing bars, and ρ_w is confinement ratio. The value of ρ_w depends on shear and axial forces and longitudinal and confining reinforcing bars.

3. Results and Discussion

In this paper, four scenarios were considered in nonlinear time history analysis of each model:1) models without considering rotational component and soil-structure interaction,2) models without considering rotational component and considering soil-structure interaction,3) models with considering rotational component and without considering soil-structure interaction, and 4) models with considering rotational component and soil-structure interaction. Table 7 lists the name of each scenario used in the nonlinear time history analysis.

Table 7. Scenario names used in the nonlinear time history analysis.

Name	Scenario
No Rocking-No SSI	Rotational component and soil-structure interaction are not considered in the analyses
No Rocking-SSI	Rotational component is not considered, but soil-structure interaction is considered in the analyses
Rocking-No SSI	Rotational component is considered, but soil-structure interaction is not considered in the analyses
Rocking-SSI	Rotational component and soil-structure interaction are considered in the analyses

3.1. Modal Analysis

Modal analysis identifies the structural dynamic characteristics. Here, periods and corresponding mode shapes during the free vibration are determined for the selected structures. It is well known that a multistory structure has multiple degrees of freedom (DOFs) and mode shapes that describe the modes of vibration for the structure in terms of relative amplitudes and angles [30] and the model shapes are typically characterized by structural properties. According to the modal analysis results, the first and third mode shapes have the greatest modal mass along

the translational x (longitudinal) and y (transverse) directions, respectively. The second mode shape appears to be the first torsional mode, and the fifth mode is the second torsional mode. The modal participation factors for 12 modes of the selected models are listed in Table 8 to 10. The tables shows the dominate direction of vibration for each of the first 12 modes.

Table 8. Modal participating mass ratios of 5-story model.

Mode	Period	UX	UY	Sum UX	Sum UY	RX	RY	RZ	Sum RX	Sum RY	Sum RZ	frequencies
1	1.325	0.7633	0	0.7633	0	0	0.2601	0	0	0.2601	0	0.755
2	1.248	0	0.7548	0.7633	0.7548	0.2693	0	0	0.2693	0.2601	0	0.801
3	1.128	0	0	0.7633	0.7548	0	0	0.7588	0.2693	0.2601	0.7588	0.887
4	0.426	0.1196	0	0.8829	0.7548	0	0.4475	0	0.2693	0.7076	0.7588	2.347
5	0.391	0	0.1232	0.8829	0.878	0.4314	0	0	0.7008	0.7076	0.7588	2.558
6	0.36	0	0	0.8829	0.878	0	0	0.1214	0.7008	0.7076	0.8802	2.776
7	0.227	0.0526	0	0.9354	0.878	0	0.1008	0	0.7008	0.8084	0.8802	4.408
8	0.203	0	0.0572	0.9354	0.9351	0.1092	0	0	0.81	0.8084	0.8802	4.927
9	0.19	0	0	0.9354	0.9351	0	0	0.0549	0.81	0.8084	0.9351	5.256
10	0.15	0.0328	0	0.9682	0.9351	0	0.1029	0	0.81	0.9113	0.9351	6.669
11	0.13	0	0.0336	0.9682	0.9688	0.1023	0	0	0.9123	0.9113	0.9351	7.712
12	0.124	0	0	0.9682	0.9688	0	0	0.0334	0.9123	0.9113	0.9685	8.057

Table 9. Modal participating mass ratios of 10-story model.

Mode	Period	UX	UY	Sum UX	Sum UY	RX	RY	RZ	Sum RX	Sum RY	Sum RZ	frequencies
1	2.636	0.7537	0	0.7537	0	0	0.255	0	0	0.255	0	0.379362671
2	2.524	0	0.7506	0.7537	0.7506	0.258	0	0	0.258	0.255	0	0.396196513
3	2.25	0	0	0.7537	0.7506	0	0	0.7498	0.258	0.255	0.7498	0.444444444
4	0.899	0.115	0	0.8687	0.7506	0	0.4251	0	0.258	0.6801	0.7498	1.112347052
5	0.848	0	0.1134	0.8687	0.864	0.4158	0	0	0.6738	0.6801	0.7498	1.179245283
6	0.766	0	0	0.8687	0.864	0	0	0.1156	0.6738	0.6801	0.8654	1.305483029
7	0.521	0.0436	0	0.9123	0.864	0	0.0664	0	0.6738	0.7465	0.8654	1.919385797
8	0.483	0	0.0446	0.9123	0.9086	0.0669	0	0	0.7408	0.7465	0.8654	2.070393375
9	0.443	0	0	0.9123	0.9086	0	0	0.0448	0.7408	0.7465	0.9102	2.257336343
10	0.354	0.0255	0	0.9378	0.9086	0	0.0795	0	0.7408	0.8261	0.9102	2.824858757
11	0.321	0	0.0261	0.9378	0.9347	0.0792	0	0	0.82	0.8261	0.9102	3.115264798
12	0.299	0	0	0.9378	0.9347	0	0	0.0261	0.82	0.8261	0.9363	3.344481605

Table 10. Modal participating mass ratios of 15-story model.

Mode	Period	UX	UY	Sum UX	Sum UY	RX	RY	RZ	Sum RX	Sum RY	Sum RZ	frequencies
1	3.86	0.7455	0	0.7455	0	0	0.2616	0	0	0.2616	0	0.2590674
2	3.737	0	0.7407	0.7455	0.7407	0.2662	0	0	0.2662	0.2616	0	0.2675943
3	3.278	0	0	0.7455	0.7407	0	0	0.74	0.2662	0.2616	0.74	0.3050641
4	1.349	0.1077	0	0.8532	0.7407	0	0.3906	0	0.2662	0.6521	0.74	0.7412898
5	1.284	0	0.1076	0.8532	0.8483	0.3824	0	0	0.6486	0.6521	0.74	0.7788162
6	1.149	0	0	0.8532	0.8483	0	0	0.1083	0.6486	0.6521	0.8483	0.870322
7	0.775	0.0459	0	0.8991	0.8483	0	0.0766	0	0.6486	0.7287	0.8483	1.2903226
8	0.732	0	0.0462	0.8991	0.8945	0.0723	0	0	0.7209	0.7287	0.8483	1.3661202
9	0.661	0	0	0.8991	0.8945	0	0	0.0473	0.7209	0.7287	0.8956	1.5128593
10	0.527	0.0239	0	0.923	0.8945	0	0.0717	0	0.7209	0.8004	0.8956	1.8975332
11	0.491	0	0.0254	0.923	0.9199	0.0734	0	0	0.7943	0.8004	0.8956	2.0366599
12	0.448	0	0	0.923	0.9199	0	0	0.025	0.7943	0.8004	0.9206	2.2321429

3.2. Nonlinear Time History Analysis

After examining the results of *OpenSees* software, averaging the outputs under the selected ground motion records by MATLAB, and converting the final outputs into the diagrams, the outcomes are presented for all 5-, 10-, and 15-storey models in selected scenarios. The considered outputs parameters include: Park and Ang damage index, column and beam plastic hinge rotation, maximum inter story drift, maximum column axial force, maximum horizontal and vertical reactions, and maximum reaction moment.

While safety against collapse is a main target, structural performance has a dominant role in the design criteria. Hence, an excessive effort has been made to reduce the damage under earthquake ground motions.

The damage index is calculated for each of the four scenarios under the selected ground motion records. The hysteretic energy is given by the area under the plot of moment vs. rotation. The results show that due to longer cycles of loading when considering SSI, the area of the hysteretic loop becomes greater comparing to no SSI considering. Hence the hysteretic energy demand is larger in former case which results in more cumulative damage in the structure.

According to Figure 7, it can be seen that the global damage index is directly proportional to the type of ground motion, i.e. rotational motion. The rotational ground motion without considering SSI effect, causes more damage than the ordinary ground motion, i.e. without considering rotational component. By looking at the results of all scenarios under the selected ground motions, it can be concluded that the earthquakes with rotational components could produce appreciable structural damage, while ordinary earthquakes considering SSI effects produce a low level of destruction.

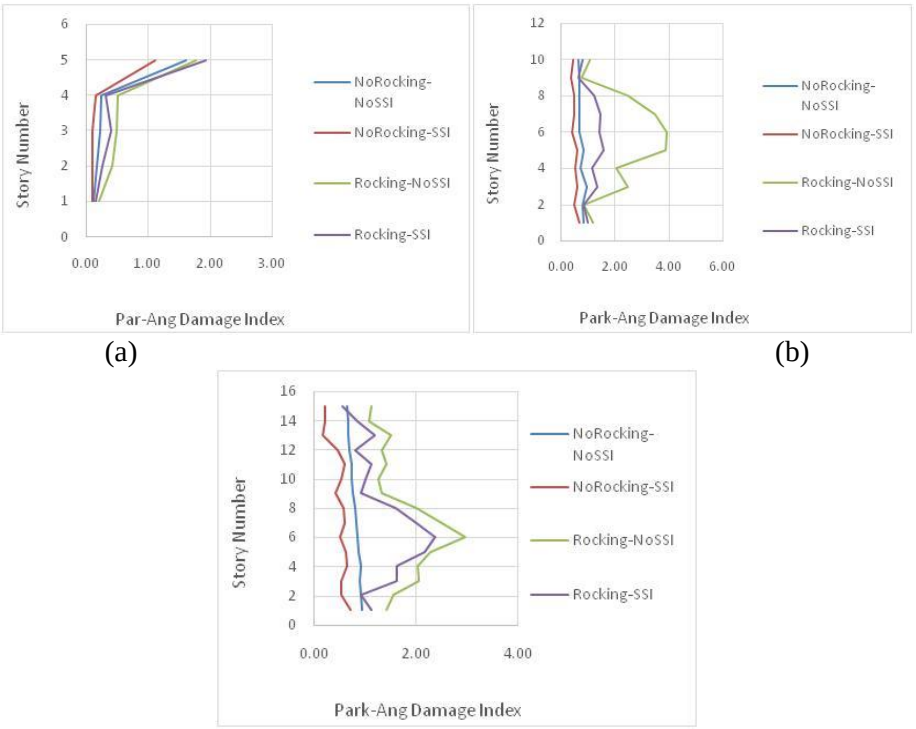

(a) (b)

(c)

Fig. 7. Park-Ang damage index of (a) 5-story model, (b) 10-story model, (c) 15 story model.

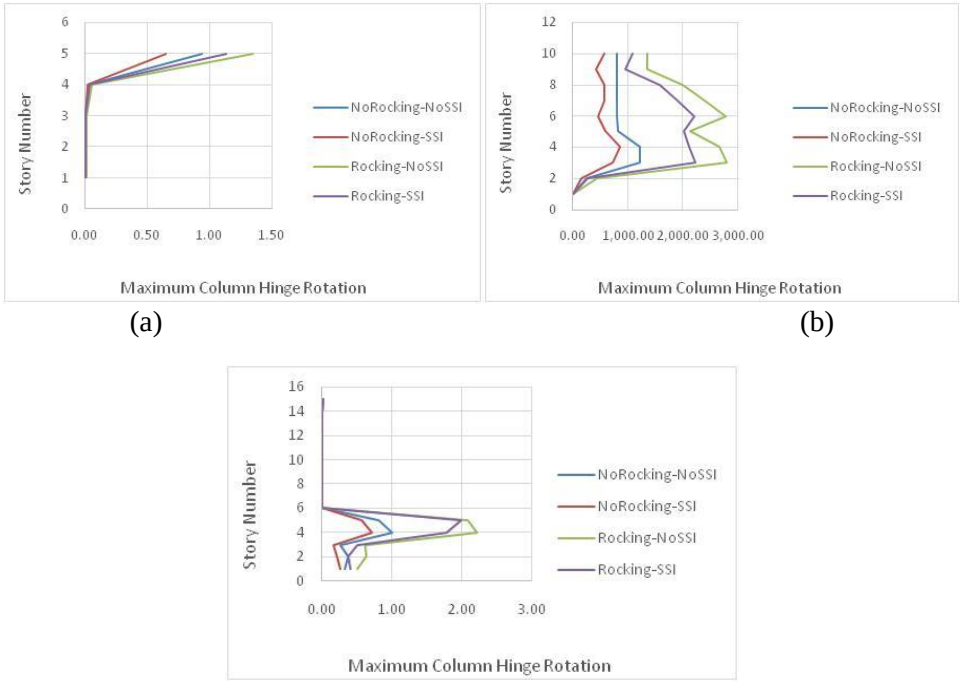

(a) (b)

(c)

Fig. 8. Maximum column hinge rotation of (a) 5-story model, (b) 10-story model, (c) 15 story model.

In addition to damage index, one of the structural damage parameters is the kinematic or cyclic ductility which can be defined in terms of rotation, curvature, or

displacement. Considering cyclic ductility as a damage measure corresponds to relating the structural collapse to maximum plastic hinge rotation, regardless of the number of plastic cycles and the amount of dissipated energy. Figures 8 and 9 indicate the maximum column and beam hinge rotation in selected scenarios. As can be seen, collapse depends on the maximum hinge rotation demand. Earthquakes with rotational components produce more hinge rotation and structural damage than ordinary earthquakes considering SSI effects.

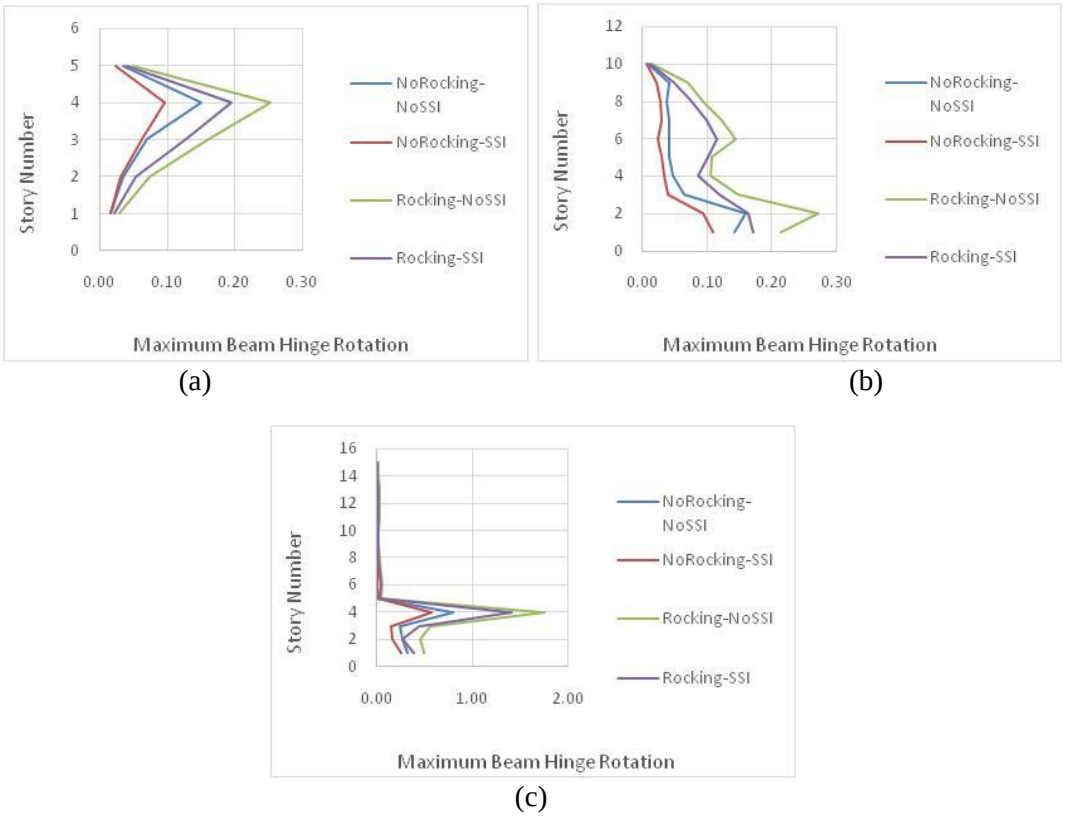

Fig. 9. Maximum beam hinge rotation of (a) 5-story model, (b) 10-story model, (c) 15 story model.

Inter storey drift demands imposed by rotational earthquake records are plotted along with the maximum column axial force to show the maximum structural response in cases of considering and not-considering rotational and SSI effect (Figure 10 and 11).

The maximum inter storey drift demand along the height for the selected models due to seven different rotational earthquake records are shown in Figure 10. For ordinary records the maximum inter storey drift demand is 1.2%, while higher values are reached when using rotational motion without considering SSI effect. For instance, the maximum inter storey drift reaches 6.4% under earthquake (2).This can be attributed to the high peak rotational velocity of the record. For record (1), the inter storey drift exceeds 7% because of the high amplitude of the rotational velocity pulse which produces high inter storey drift demands.

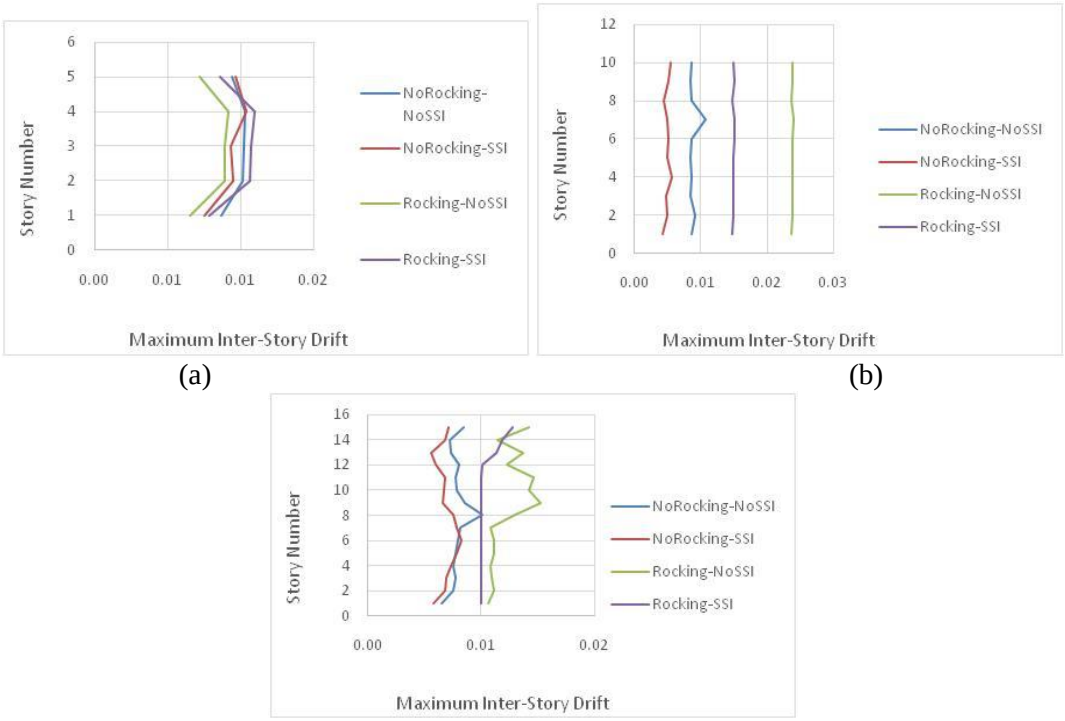

Fig. 10. Maximum inter story drift of (a) 5-story model, (b) 10-story model, (c) 15 story model.

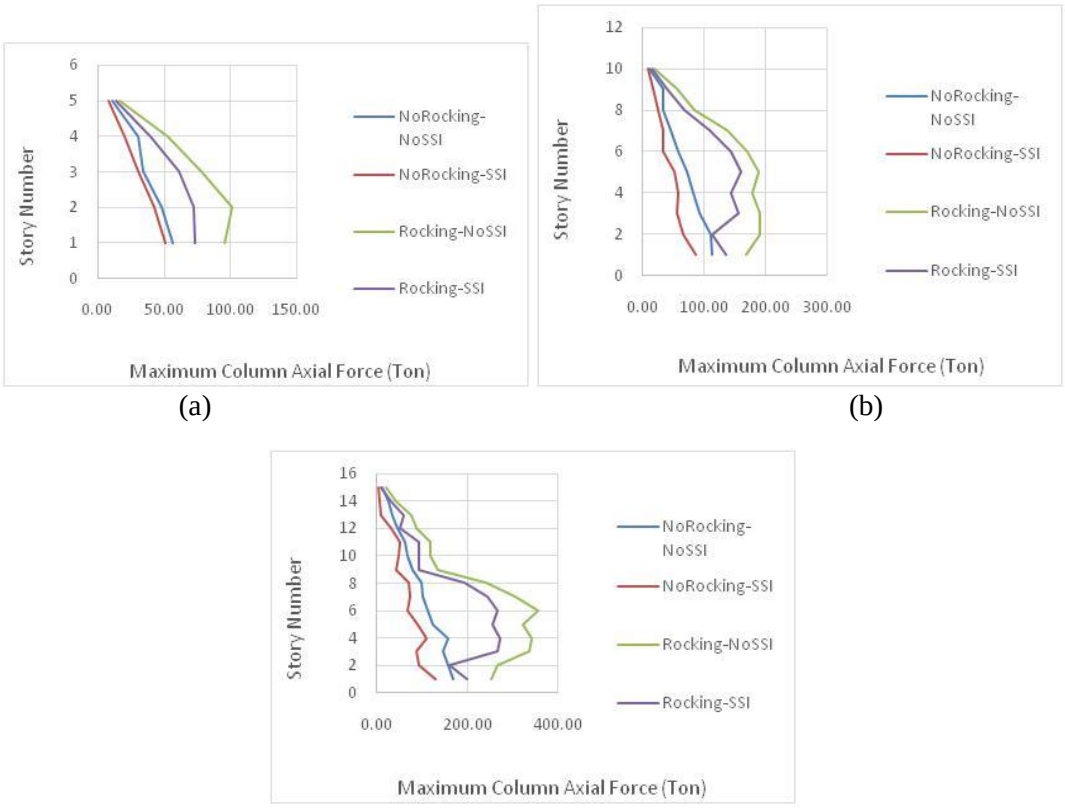

Fig. 11. Maximum column axial force of (a) 5-story model, (b) 10-story model, (c) 15 story model.

Itcan be seen from figure 11 that the maximum interstory drift ratio (IDR) shifts from the upper half to the lowerhalf of buildings with increase in lateral stiffness ratio. The average IDR under rotational ground motions is greater than those under non-rotational ground motions. Figures 12 to 14 illustratethemaximum horizontal and vertical reaction force and moment of selected models, respectively. From the response of various models shown in figures 12 to 14, it can be observed that thecorresponding response of models under rotational earthquake records is much higher than that of ordinary record. The results show that due to high stiffness of low-rise models, the structural response is expected to be dominated by the first mode of vibration. The results of this research work are consistent with other research in the same condition. For example, Hassani et al. [31] observed that SSI increases the inelastic displacement ratios with exception of very short period structures. Nakhaei and Ghannad [32] also concluded that the SSI substantially increases the damage index of short-period buildings located on soft soils. Increasing the aspect ratio of the structure can increase this effect.

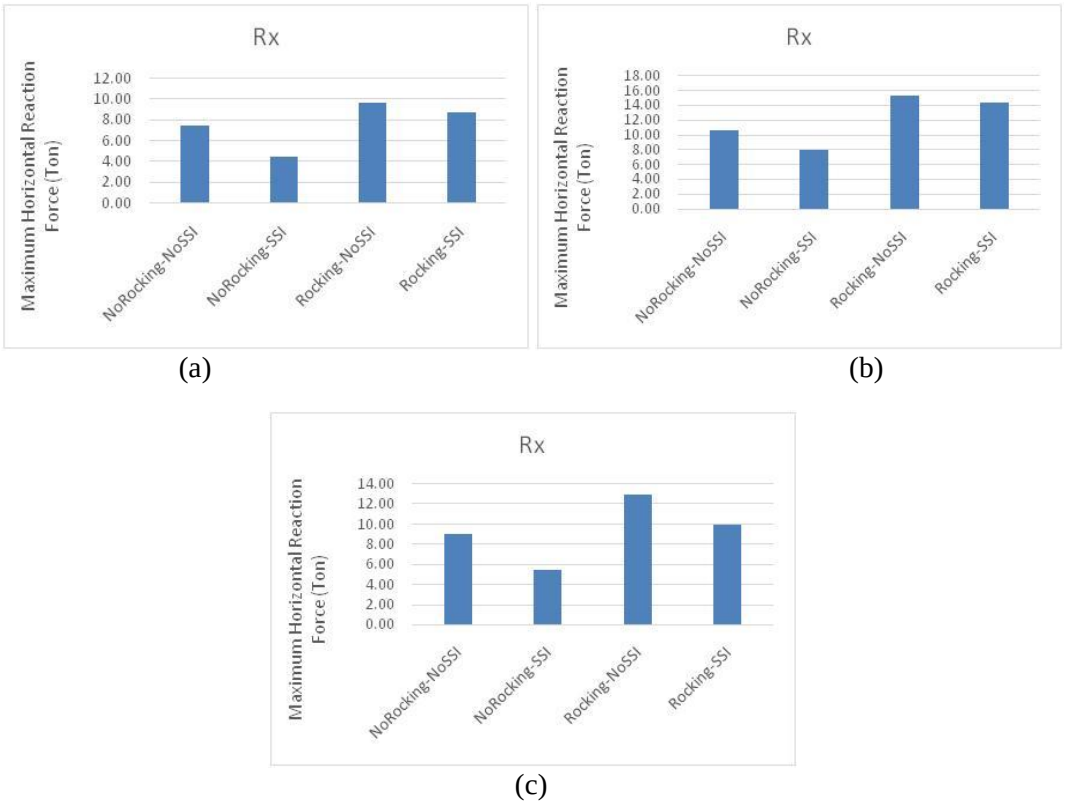

Fig 12. Maximum horizontal reaction force of (a) 5-story model, (b) 10-story model, (c) 15 story model.

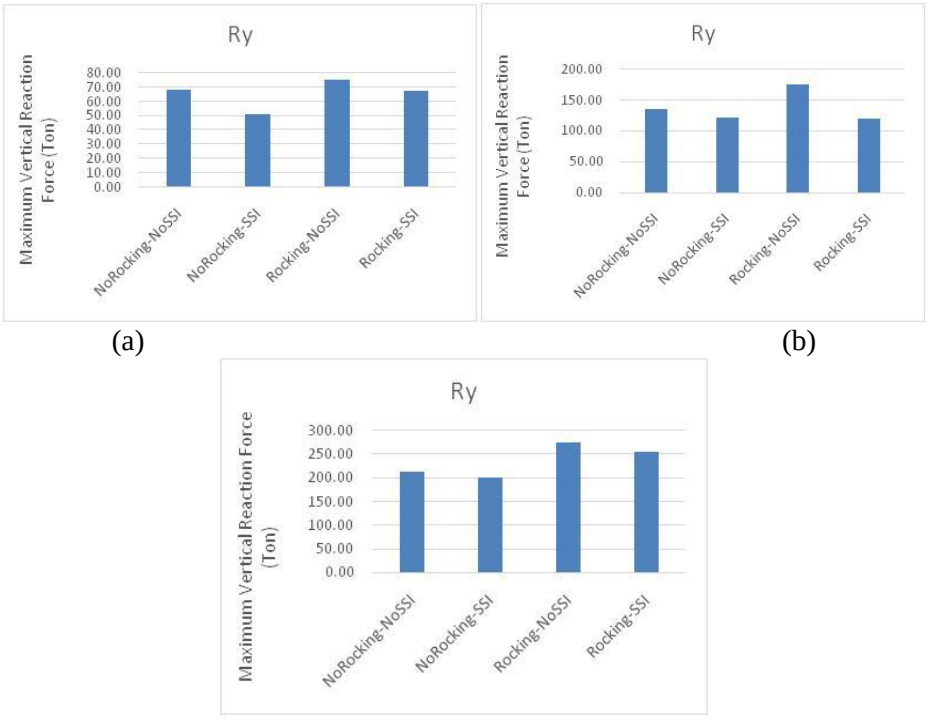

Fig. 13. Maximum vertical reaction force of (a) 5-story model, (b) 10-story model, (c) 15 story model.

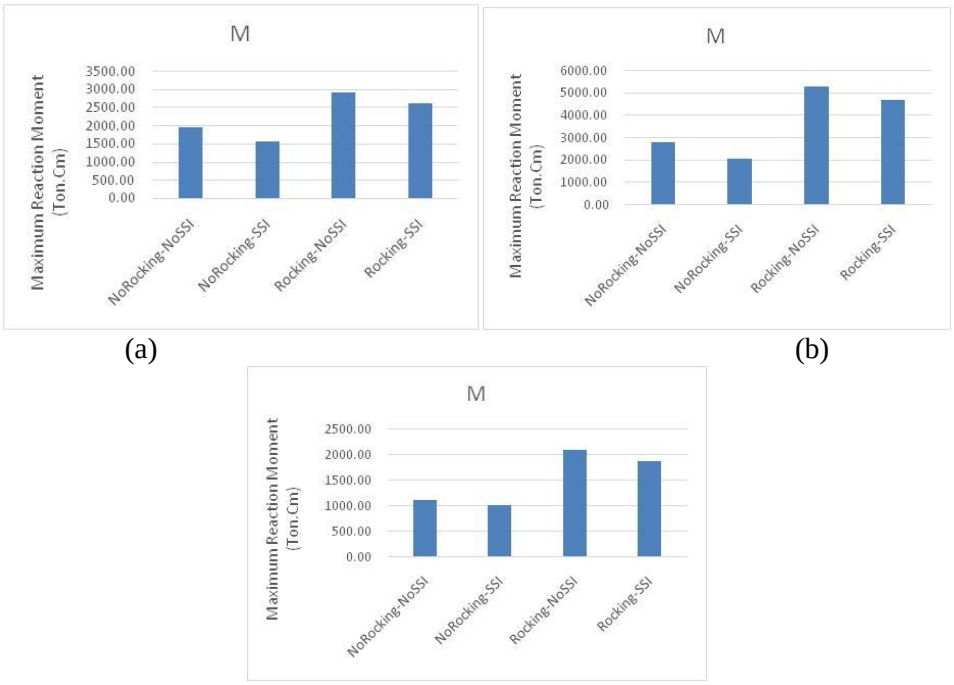

Fig. 14. Maximum reaction moment of (a) 5-story model, (b) 10-story model, (c) 15 story model.

4. Conclusion

Typical seismic design and performance assessment do not take into account the rotational motions. The contribution of rocking and horizontal component to the structural response is significant. This paper used seven accelerograms having rotational

components to evaluate seismic damage indices in RC buildings. The considered RC buildings which designed as per intermediate moment-resisting frame system were analyzed using *OpenSees* in nonlinear dynamic domain. The findings of the present study are concluded as following:

- The rotational ground motion without considering SSI effect causes more damage than the ordinary ground motion, i.e. without considering rotational component.

- Earthquakes with rotational components produce more hinge rotation and structural damage, while ordinary earthquakes considering SSI effects yield lower values.

- For ordinary records, the maximum inter storey drift demand (IDR) is 1.2%, while higher values are observed when using rotational motion without considering SSI effect i.e. 7%.

- Maximum IDR, shifts from the upper half to the lower half of buildings as the lateral stiffness ratio increases.

- The average IDR under rotational ground motions is greater than those under non-rotational ground motions.

- Inclusion of soil-structure interaction in the modeling results inless damage response in most of the studied models.

REFERENCES

[1] Richter, C. F. (1958). Elementary seismology, W. H. Freeman and Company, San Francisco.

[2] Aki, K., Richards, P. G. (1980). Quantitative seismology, First Ed., W. H. Freeman and Company, San Francisco.

[3] Aki, K., Richards, P. G. (2002). Quantitative seismology, Second Ed., University Science Books, Sausalito.

[4] Nigbor, R. L. (1994). Six-degree-of-freedom ground motion measurement, Bulletin of the Seismological Society of America, 84(5): 1665–1669.

[5] Takeo, M. (1998). Ground rotational motions recorded in near-source region of earthquakes, Geophysical Research Letters, 25(6): 789–792.

[6] Lee, W. H. K., Shin, T.C., Kuo, K.W., Chen, K.C., Wu, C.F. (2001). CWB free-field strong-motion data from the 21 September Chi-Chi, Taiwan, earthquake, Bulletin of the Seismological Society of America, 91(5): 1370–1376.

[7] Huang, B. S. (2003). Ground rotational motions of the 1991 Chi-Chi, Taiwan earthquake as inferred from dense array observations, Geophysical Research Letters, 30(6): 1307–1310.

[8] Liu, C.C., Huang, B.S., Lee, W.H.K., Lin, C.J. (2009). Observing rotational and translational ground motionsat the HGSD station in Taiwan from 2007 to 2008, Bulletin of the Seismological Society of America, 99(2B): 1228-1236.

[9] Falamarz-Sheikhabadi, M.R. (2014) Simplified relations for the application of rotational components to seismic design codes, Engineering Structures, 59: 141-152.

[10] Basu, D., Whittaker, A.S., Constantinou, C. (2015) Characterizing rotational components of earthquake ground motion using a surface distribution method and response of sample structures, Engineering Structures, 99: 685-707.

[11] Singla, V.K., Gupta, V.K. (2016). On planar seismic wavefront modeling for estimating rotational ground motions: Case of 2-D SH line-source, Soil Dynamics and Earthquake Engineering, 85: 62-77.

[12] Falamarz-Sheikhabadi, M.R., Ghafory-Ashtiany, M. (2015). Rotational components in structural loading, Soil Dynamics and Earthquake Engineering, 75: 220-233.

[13] Rodda, G. K., & Basu, D. (2019). On Conditional Simulation of Spatially Varying Rotational Ground

Motion. Journal of Earthquake Engineering, 1-36.

[14] Vicencio, F., & Alexander, N. A. (2019). A parametric study on the effect of rotational ground motions on building structural responses. Soil Dynamics and Earthquake Engineering, 118, 191-206.

[15] Tajammolian, H., Khoshnoudian, F., & Loghman, V. (2017). Rotational components of near-fault earthquakes effects on triple concave friction pendulum base-isolated asymmetric structures. Engineering Structures, 142, 110-127.

[16] Nazarov, Y. P., Poznyak, E., & Filimonov, A. V. (2015). A brief theory and computing of seismic ground rotations for structural analyses. Soil Dynamics and Earthquake Engineering, 71, 31-41.

[17] Iranian Code of Practice for Seismic Resistant Design of Buildings. 2015. Standard NO. 2800-15, Building and Housing Research Center,4rd edition.

[18] National building regulations, part 9: Design and construction of RC buildings. (2013) Ministry of Housing and Urban Development, Office of National Building Regulations, Tehran, Iran.

[19] CSI Reference Manual for ETABS2000; Computers and Structures, Inc.: Berkeley, CA, USA, 2015.

[20] Mortezaei, A., Ronagh, H.R., Kheyroddin, A., GhodratiAmiri, G. (2011). Effectiveness of modified pushover analysis procedure for the estimation of seismic demands of buildings subjected to near-fault earthquakes having forward directivity. The Structural Design of Tall and Special Buildings, 20(6): 679-699.

[21] OpenSees, 2016, http://opensees.berkeley.edu/

[22] Altoontash, A. (2004). Simulation and damage models for performance assessment of reinforced concrete beam-column joints, Ph.D. Thesis, Stanford University.

[23] Ibarra, L.F., Medina, R.A., Krwinkler, H. (2005). Hysteretic models that incorporate strength and stiffness deterioration, Earthquake Engineering and Structural Dynamics, 34: 1489–1511

[24] Haselton, C.B., Liel, A.B., Lange, S.T., Deierlein, G.G. (2007). Beam-column element model calibrated for predicting flexural response leading to global collapse of RC frame buildings, PEER 2007/03 Report, Pacific Earthquake Engineering Research Center.

[25] Wolf JP, Deeks AJ. Foundation vibration analysis: a strength of materials approach. Amsterdam: Elsevier; 2004.

[26] ATC. Seismic Evaluation and Retrofit of Concrete Buildings, ATC- 40 Report, Volumes 1 and 2, Applied Technology Council, Redwood City, California, 1996.

[27] Park, Y.J., Ang, A.H.S. (1985). Mechanistic seismic damage model for reinforced concrete, Journal of Structural Division, ASCE 111(4): 722–739.

[28] Kheyroddin, A. Mortezaei, A. (2008). The effect of element size and plastic hinge characteristics on nonlinear analysis of RC frames. Iranian Journal of Science & Technology, Transaction B, Engineering, 32(B5): 451-470.

[29] Kunnath S.K., Reinhorn, A.M., Lobo, R.F. (1992). IDARC Version 3.0: A program for the inelastic damage analysis of reinforced concrete structures. Report No. NCEER-92-0022, National Center for Earthquake Engineering Research, State University of New York at Buffalo.

[30] Soleymani, A., Safi, M. (2014). Estimation of interdependencies between seismic parameters and damage indices including the MFDR model and the modified Park-Ang model, Journal of Seismology and Earthquake Engineering (JSEE), 16(1): 71-79.

[31] Hassani, N., Bararnia, M., & Amiri, G. G. (2018). Effect of soil-structure interaction on inelastic displacement ratios of degrading structures. Soil Dynamics and Earthquake Engineering, 104, 75-87.

[32] Nakhaei, M., & Ghannad, M. A. (2008). The effect of soil–structure interaction on damage index of buildings. Engineering Structures, 30(6), 1491-1499.